Journal of Petroleum Science and Engineering 220 (2023) 111163

Contents lists available at ScienceDirect

Journal of Petroleum Science and Engineering

journal homepage: www.elsevier.com/locate/petrol

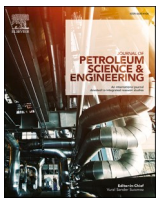

# Finite element analysis of drill pipe-slip system

Liping Tang [a,b], Baolin Guo [a], Marcin Kapitaniak [b], Vahid Vaziri [b], Marian Wiercigroch [b,*]

[a] School of Mechatronic Engineering, Southwest Petroleum University, Chengdu, 610500, PR China
[b] Centre for Applied Dynamics Research, School of Engineering, University of Aberdeen, Aberdeen, AB24 3UE, UK

ARTICLE INFO

*Keywords:*
Drill-pipe
Slip insert
Friction
Stress distribution
Finite element analysis

ABSTRACT

As an important tool for tripping of a drill-string, a drill-pipe (DP)-slip system directly affects both the service life of a DP and the target depth it can reach. In this paper, a finite element (FE) model programmed in ABAQUS is used to simulate interactions within a DP-slip system. For this model, materials, geometric dimensions, loads, and boundary conditions were determined from an actual DP-slip system. A special attention has been paid on the stress field of the slip insert and the DP focusing on the geometric parameter optimization of the slip insert with regards to the stress distribution, wherein factors like a longitudinal groove number in slip insert, a number of slip inserts, and a number of row spacing of slip inserts are considered. Numerical results show that the circumferential stress distribution and stress distribution in the direction of DP axis change for both the DP and slip insert and that the stresses of the inner surfaces are higher than that of the outer surfaces. Effects of geometric parameters of the slip insert on the stress distributions of both DP and slip insert are studied and the corresponding optimized values are obtained, which can be used when designing slip insert tools.

## 1. Introduction

Energy resources are a fundamental driving force towards a country's continuous development and progress, and the development of several countries depends on the control of such energy sources (Zaman and Moemen, 2017; Sikder et al., 2019). Oil and gas are the most widely used energy resources, and their development and utilization are important indicators of a country's economic strength (Adeosun et al., 2022). With the continuous depletion of shallow oil and gas resources in recent years, conventional oil and gas discoveries have continued to decline around the world, and drilling operations have significantly decreased. As a result, the exploration and development of unconventional oil and gas sources has gradually emerged, and drilling has gradually shifted to deeper onshore and offshore resources (Falcone et al., 2018; Li et al., 2018; Ali et al., 2020; Liu, 2021). Constructing oil wells in harsh geological conditions is a technical challenge for the petroleum industry as it poses considerable threats to innovative drilling technologies (Hill et al., 2004; Jarski et al., 2011; Bordet et al., 2016; Sun et al., 2016; Tomac and Sauter, 2018). One of the key technologies for drilling deep resources is how to lift a drill-pipe (DP) to the wellhead or lower it to a designated position of the wellbore (Amezaga et al., 2014).

The DP acts as a bridge in wellbore drilling that connects the ground level with the underground. The mechanical properties of DPs are important for safe and efficient drilling operations (Zamani et al., 2016; Li et al., 2017; Belkacem et al., 2019; Chang et al., 2021; Liu et al., 2022). During drilling operations, the task of lifting or lowering the DPs is generally completed with hanging or supporting devices, such as an elevator or slip (Sathuvalli et al., 2002; Awad et al., 2019). Slips are widely used in the petroleum industry because of their convenience, good applicability, and easy realization of mechanical lifting of DPs (Verhoef and Rijzingen, 2015). A typical slip system is composed of three parts: (a) slip inserts that have jagged curves that bite into the outer DP surface, (b) slip bodies with tapered outer surfaces used to fit with the rotary table, and (c) attached parts such as connecting elements and controlling units (Brock et al., 2007). For a slip system, the slip inserts are fixed into the slip bodies but can be replaced when they fail.

Fig. 1(a) shows a slip system that is commonly used to interact with DPs in drilling operations. Under the DP axial load, the DP drives the slip bodies downwards using frictional forces. As the slip bodies move, they exert a radial force on the DP to clamp it. In this way, the slip inserts support the DP by embedding slightly into its outer surface when they are fully engaged (Flores et al., 2015; Jarski et al., 2011). It was found by examining DPs used in real situations that die marks appear on the outer surface of the DP (shown in Fig. 1(b)), which may cause necking or even fractures leading to DP failures (Lu et al., 2005; Moradi and Ranjbar,

* Corresponding author.
*E-mail address:* m.wiercigroch@abdn.ac.uk (M. Wiercigroch).

https://doi.org/10.1016/j.petrol.2022.111163
Received 20 April 2022; Received in revised form 2 October 2022; Accepted 23 October 2022
Available online 28 October 2022

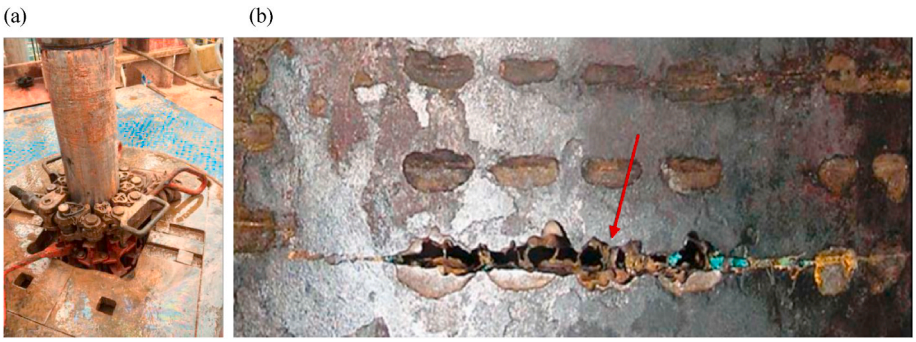


**Fig. 1.** (a) A schematic view showing the DP-slip system, where the slip is installed in the rotary table and used to suspend the DP; (b) Example of DP failure due to action of the slip inserts, where permanent die marks are shown on the external surface of the DP body and corrosion perforation (shown by the arrow) appears due to the die marks. Adopted from Albdiry and Almensory (2016).

$$F_{crush} = F_{yield}\sqrt{\frac{2}{1+\left[1+\frac{KD}{2L}\right]^2+\left[\frac{KD}{2L}\right]^2}}. \tag{1}$$

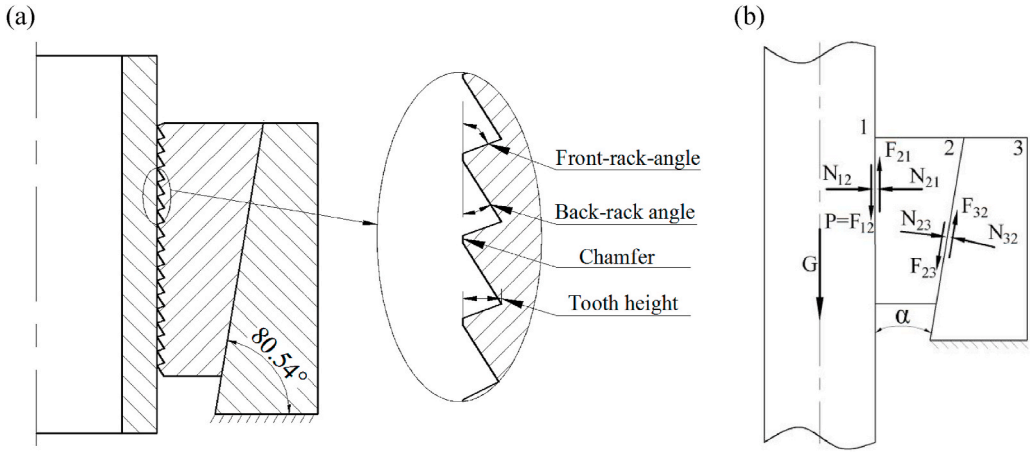


**Fig. 2.** Schematic of the DP-slip system; (a) Longitudinal profile of the DP-slip system which includes a DP, a slip and a rotary table, where the slip is a combination of slip insert and slip body because the slip insert is fixed into the slip body for an actual slip system; (b) Force diagram in the DP-slip system depicting gravitational ($G$), normal ($N_{ij}$) and frictional forces ($F_{ij}$).

2009; Albdiry and Almensory, 2016; Damjanović et al., 2019; Santus et al., 2020). A DP failure not only creates significant safety hazards, but also reduces the drilling efficiency and consequently increases the drilling costs (Liu et al., 2016). These types of accidents can be avoided however with using robust designs which are supported by predictive numerical models. Hence, it is important to investigate the mechanical behavior of DPs when using slip systems in order to implement effective preventive measures that reduce the probability of DP failures (Hill et al., 2004; Simpson et al., 2005; Dao and Sellami, 2012).

Several works have explored the reasons for the high probability of failure of DPs in the contact area with the slip. Reinhold and Spiri (1959) first discovered the DP failure problem with slips and DP contact area through a bidirectional load in the slip area. They derived a formula for the slip crushing load $F_{crush}$, using a "$K$-factor" to describe the relationship between the transverse shear force of the slip and the axial force on the DP,

$$K = \frac{F_T}{F_A} = \frac{1-\mu_{BS}\tan\theta}{\mu_{BS}+\tan\theta}, \tag{2}$$

where $F_{yield}$ is the yield force of the DP, $D$ is the outer diameter of the DP, $L$ is the axial length of the slip area, $F_A$ is the axial load, $F_T$ is the tangential load, $\mu_{BS}$ is the frictional coefficient between the slip body and the rotary table, and $\theta$ is the tapered angle of the slip body, which is standardized by the American Petroleum Institute (API) as 9°27′45″. Subsequently, Vreeland (1961) designed eight sets of meticulous experiments for the grade E DP (outer diameter of 127 mm, which is 5 inches) loaded with standard and extended length manual slips.

The experimental results were compared with the Reinhold-Spiri predictions of Equation (1), which indicated the experimental results agree well with the predicted values. However, using the Reinhold-Spiri formula to calculate the yield load of the DP is non-conservative based on the recent research by Payne et al. (2005), because the initial yield of the DP inner diameter is approximately 20% lower than that predicted by Equation (1). After the studies by Reinhold and Spiri and by Vreeland, it was not until 1985 that the analysis of slip crushing restarted. Hayatdavoudi (1985) discussed the design criteria of slips to reduce a possibility of DP yielding. The data indicated that the deformation of the DP inner diameter above the slip is larger than that near the slip. In 1999, Rahman et al. (1999a, b) developed an approach for fatigue analysis of DPs, where the alternating bending stress due to dogleg, the axial stress due to the weight of a drill-string, and stress concentration due to die marks, are included in the analysis. In 2002, a study by Sathuvalli et al. (2002) reported a large number of available experimental data on slip crushing, which also indicated differences between the experimental results and those from the Reinhold-Spiri model. They

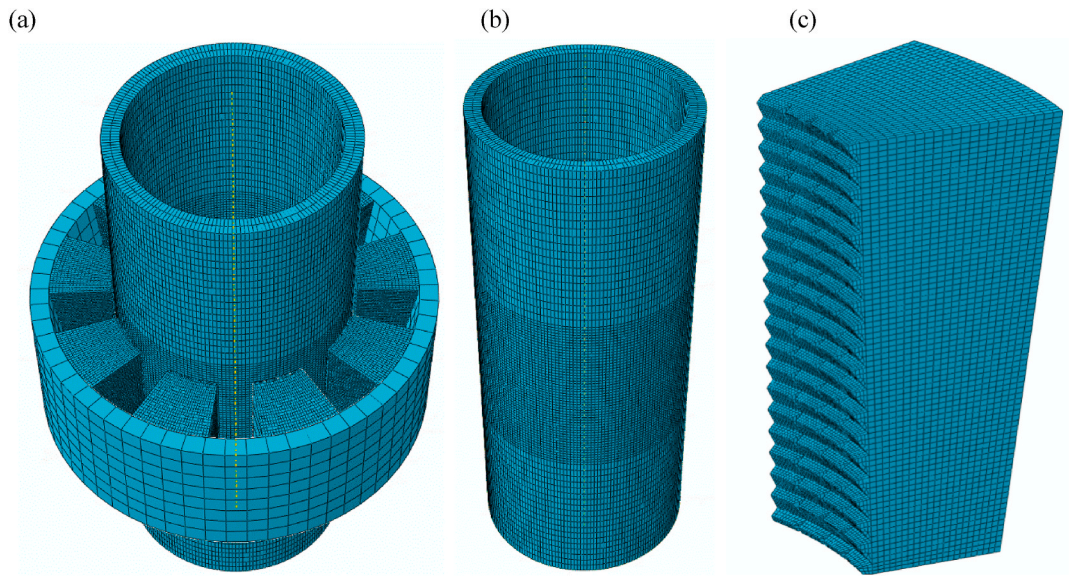


**Fig. 3.** FE model for the DP-slip system; (a) Global model includes rotary table, slips and DP; (b) A meshed DP with the section contact with the slip inserts is refined to improve the accuracy of the numerical simulation; and (c) A meshed slip insert with the teeth that contact with the DP are refined.

**Table 1**
Boundary conditions for rotary table, DP and slip inserts in two steps.

| Steps | Initial | Step 1 | Step 2 |
|---|---|---|---|
| Rotary table | Fixed | Fixed | Fixed |
| DP | Free | Fixed | Free |
| Slip inserts | Free | Free | Free |

**Table 2**
Loads for slip inserts and DP in two steps.

| Loads | Initial | Step 1 | Step 2 |
|---|---|---|---|
| Slip | Not loaded | 1 MPa (downward) | Not loaded |
| DP | Not loaded | Not loaded | 88.11 MPa (downward) |

**Table 3**
Mechanical properties of the steels used for DP-slip system.

| Mechanical properties of 20CrMnMo (steel for DP and rotary table) | Value |
|---|---|
| Density | 7870 kg/m$^3$ |
| Poisson's ratio | 0.254 |
| Young's modulus | 207 GPa |
| Yield strength | 885 MPa |
| Tensile strength | 1185 MPa |
| **Mechanical properties of 20CrMnTi (steel for slip inserts)** | **Value** |
| Density | 7870 kg/m$^3$ |
| Poisson's ratio | 0.254 |
| Young's modulus | 207 GPa |
| Yield strength | 835 MPa |
| Tensile strength | 1080 MPa |

developed a modified equation for the slip crushing load by establishing a more accurate slip crushing model by describing the slip loading mechanism in a more detail based on the analysis of Reinhold and Spiri.

After reviewing and analyzing the existing literature, it has been understood that the current efforts are focused on calculating the slip crushing load or the clamping limits of the slip (Zhang et al., 2010; Tikhonov et al., 2017; Paslay et al., 2006), whereas the sensitivity of the slip insert structure and geometric parameters has rarely been analyzed. Since the slip insert creates permanent die marks on the DP, the structure of the slip insert is of great importance (Hossain et al., 1998; Bordet et al., 2016). However, the cost for carrying out experimental tests for the purpose of optimizing the structure of slip insert is almost prohibitive, as it requires the multiscale high fidelity computations using Finite Element Methods (FEMs) (see e.g. Shahani and Sharifi, 2009; Feng and Qian, 2020; Zhang and Zhu, 2020). In 2016 and 2020, Tang et al. (2016, 2020) proposed a FE model of the DP-slip system to study the effects of structural parameters on mechanical performance, including rake angles, tooth height, and tooth chamfer. However, there are still many other factors seem to influence the mechanical performance, such as number of slip inserts, longitudinal groove number of slip inserts, and row spacing of the slip insert. Therefore, a detailed modelling and a focused FE analysis related to a typical DP-slip system are carried out here with a view to find new insights.

The structure of this paper is as follows. In Section 2, the mechanical model of the DP-slip system is presented and supported by mathematical modelling of the static equilibria. As a next step, in Section 3, a FE model is developed in the parameter values are determined by referring to the drilling system used in a real drilling application, which is followed by the FE modelling and analysis of the mechanical behaviour of the considered system focusing on the resulting stress fields. In Section 4, parameter sensitivity analysis on the slip insert is conducted, including a longitudinal groove number of slip inserts, a number of slip inserts, and row spacing of slip inserts. Finally, conclusions are drawn in Section 5.

## 2. Mechanical model of the DP-slip system

In order to study the mechanical behavior of the DP-slip system, a mechanical model of the system (Fig. 2) is developed. As seen in Fig. 2, the system includes a DP, a slip, and a rotary table. Usually, a slip system contains a number of slip inserts and a slip body, where the slip inserts are fixed into the slip body. In this way, engineers just need to replace the slip inserts rather than replace the whole slip system. According to this real characteristic of the slip system, the slip in this model is represented as a combination of slip inserts and a slip body. For the slip, the slip inserts bite into the outer surface of DP and the slip body contact with the rotary table through its tapered surface. In this section, the mechanical model presented is used to discuss the forces of the system in an equilibrium state and the corresponding stress of both slip insert and DP.

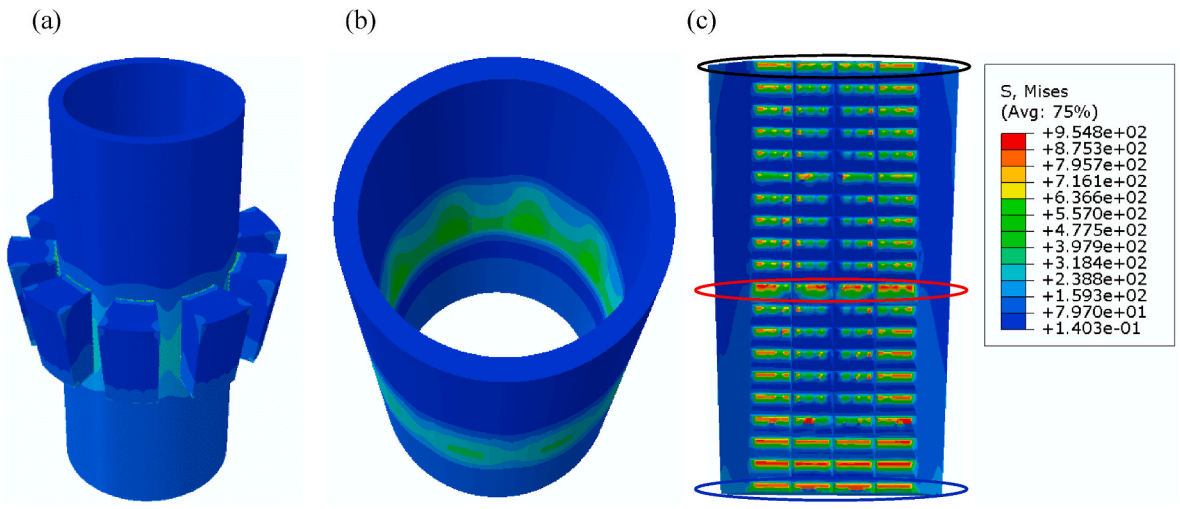


**Fig. 4.** Stress of DP-slip system, for the parameter values: front rake angle 75°, back rake angle 35°, tooth height 2 mm, and the chamfer 0.2 mm, (a) General stress state of the entire system, (b) Stress distribution of the DP showing the stress of the inner surface is higher than that of the outer surface, which is agree with the theoretical analysis, and (c) Stress distribution of the slip insert showing peak stress occurs at the end of the slip insert. (Units: MPa).

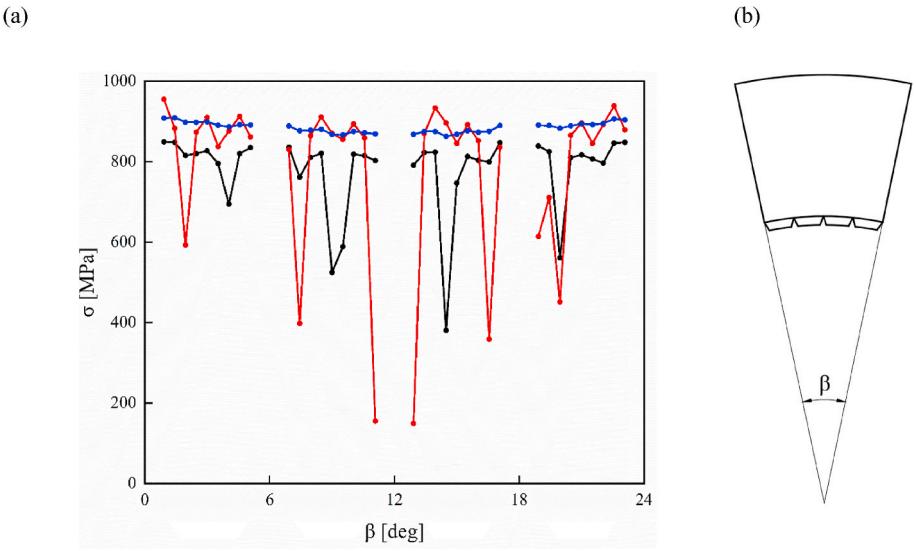


**Fig. 5.** (a) Stress σ distribution in three positions of the slip inserts shown in Fig. 4(c) at the upper end of the contact section (in black), middle of the contact section (in red), and lower end of the contact section (in blue). In general, the lower ends of the slip insert exhibit the highest stresses. (b) Definition of angle β. (For interpretation of the references to colour in this figure legend, the reader is referred to the Web version of this article.)

### 2.1. Frictional coefficient in the DP-slip system

As seen from Fig. 2, when the DP moves downwards under an axial load, a relative motion occurs between the DP and the slip insert, as well as between the slip body and the rotary table. When the DP is clamped by the slip, the DP-slip system is in an equilibrium state that satisfies the following equations:

$$\begin{cases} N_{12} + F_{32}\sin\alpha - N_{32}\cos\alpha = 0 \\ F_{12} - F_{32}\cos\alpha - N_{32}\sin\alpha = 0 \end{cases}, \tag{3}$$

where the friction $F_{32}$ and normal force $N_{32}$ are related via the Coulomb friction law:

$$F_{32} = N_{32}\mu_1. \tag{4}$$

By substituting Equation (4) into Equation (3), the following expression is obtained:

$$N_{12} = F_{12}\frac{1-\mu_1\tan\alpha}{\mu_1+\tan\alpha}, \tag{5}$$

where $F_{12}$ is the frictional force between the slip inserts and the DP, $N_{12}$ and $N_{21}$ is a pair of radial forces between the slip body and the DP, $N_{32}$ is the reaction force of the rotary table on the slip body, $F_{32}$ and $\mu_1$ are the frictional force and frictional coefficient between the slip body and rotary table, respectively, and $\alpha$ is the taper bevel angle of the slip body as standardized by the API. As seen from Equation (5), the radial force $N_{12}$ on the DP is proportional to the axial load $P$ and $\frac{1-\mu_1\tan\alpha}{\mu_1+\tan\alpha}$. Moreover, $\frac{1-\mu_1\tan\alpha}{\mu_1+\tan\alpha}$ decreases with greater $\mu_1$, indicating a larger radial load $N_{12}$ is obtained at a smaller $\mu_1$. Therefore, the frictional coefficient between the slip body and the rotary table should be as large as possible to reduce the radial load. Assuming all inserts are taking an equal load, $P = \frac{G}{n}$, where $n$ is a number of slip inserts.

When a slip system is in operation, it may not be possible to tightly clamp the DP due to the slippage. Therefore, the slip inserts can cause a

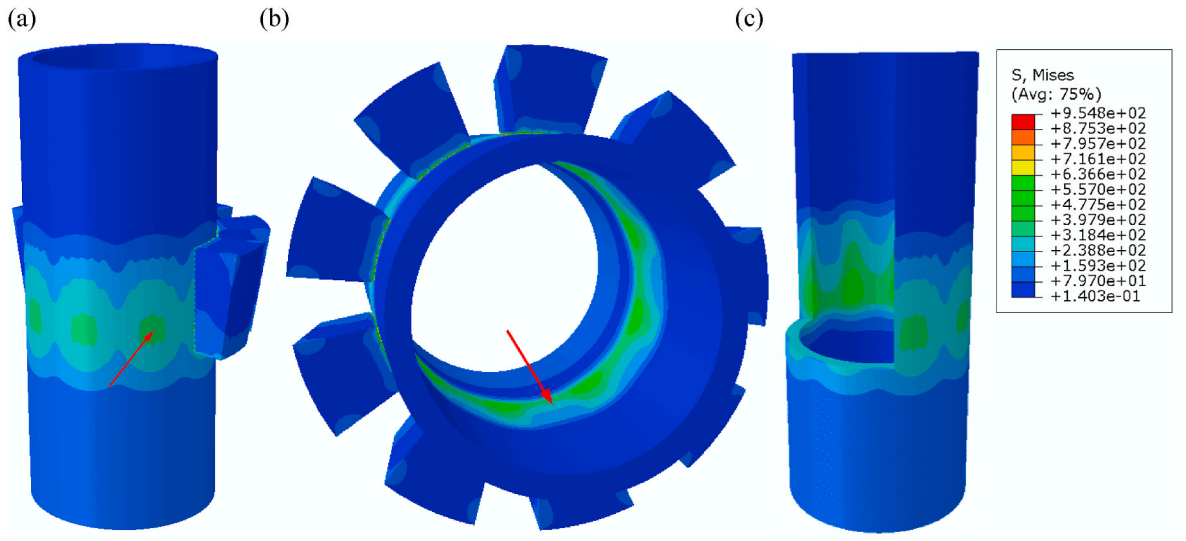


**Fig. 6.** Comparison of the stress distribution between the outer surface and the inner surface of the DP in the contact region, showing the maximum stress on the outer surface of the DP occurs in the region where the slip inserts contact the DP while the peak stress on the inner surface corresponds to the gap between each two slip inserts. (a) Stress distribution of the outer surface, (b) Stress distribution of the inner surface, and (c) Sectional view of the stress distribution (Units: MPa).

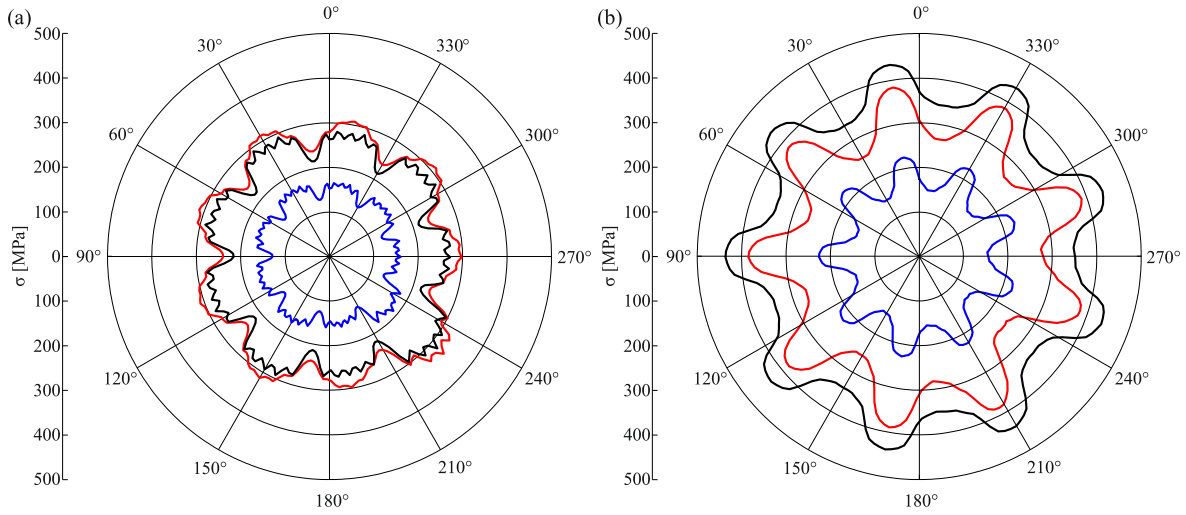


**Fig. 7.** The stress distribution for three contact positions of the outer surface and inner surface of the DP: upper contact section (blue curve), middle contact section (red curve), and lower contact section (black curve). For both outer surface (a) and inner surface (b) stress of the upper contact section is the lowest. For the outer surface, stress of the middle contact section is higher than that of the lower contact section while the inner surface behaviors the opposite. (Units: MPa). (For interpretation of the references to colour in this figure legend, the reader is referred to the Web version of this article.)

significant damage to the DP surface. Consequently, it is necessary to explore the conditions under which the slip system can clamp the DP. Assuming that the frictional coefficient between the slip inserts and the DP is $\mu_2$, the frictional force between them is given as:

$$F_{12} = F_{21} = \mu_2 N_{12}, \tag{6}$$

To ensure the DP is effectively clamped by the slip system, the following condition must be met:

$$F_{12} \geq P, \tag{7}$$

where $P$ is the axial load of the DP supported by each of slip inserts. Combining Equations (5)–(7) leads to the following formula:

$$\mu_2 \geq \frac{\mu_1 + \tan\alpha}{1 - \mu_1 \tan\alpha}. \tag{8}$$

As can be deduced from Equation (8), $\mu_2$ is proportional to $\mu_1$. A large value of $\mu_2$ is seen for large $\mu_1$, which increases the probability of DP slippage. Therefore, the value of $\mu_1$ is critical to ensure that the DP can be clamped while also receiving a small radial force.

### 2.2. Stress analysis of DP in slip system

When a DP is held by a slip system, it can be regarded as a thick-walled cylinder under a uniform external pressure due to its large length-diameter ratio, when the yield occurs, it satisfies the following equation:

$$(\sigma_1 - \sigma_r)^2 + (\sigma_1 - \sigma_\varphi)^2 + (\sigma_r - \sigma_\varphi)^2 = 2\sigma_s^2, \tag{9}$$

where $\sigma_s$ is the DP yield strength, $\sigma_1$ is the DP axial stress, and $S_P$ is the DP cross-sectional area:

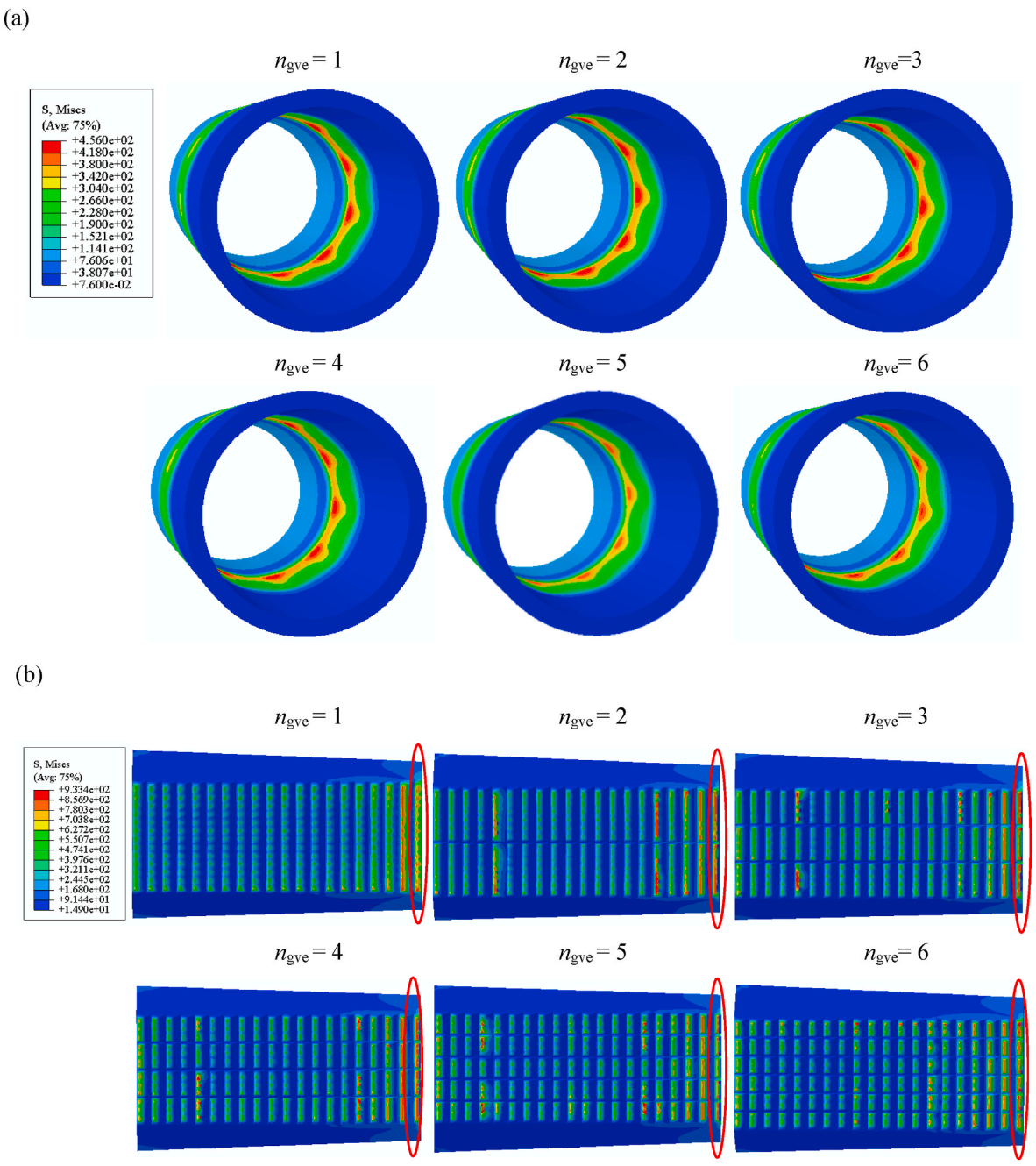


**Fig. 8.** Stress distributions of the DP and slip insert with respect to the number of longitudinal grooves, $n_{gve}$, which changes from 0 to 5: (a) DP and (b) Slip insert. For the 6 cases, the stress of the DP decreases and then increases, and the stress of the slip insert seems to increase with increasing the longitudinal groove number but with small increment. (Units: MPa).

$$\sigma_1 = \frac{G}{S_P}. \tag{10}$$

The Lame formulas (Boresi and Chong, 2011) are applied to obtain the radial stress $\sigma_r$ and hoop stress $\sigma_\varphi$ of the DP when subjected to a uniform external pressure as:

$$\sigma_r(\rho) = -\frac{1-\frac{d^2}{\rho^2}}{1-\frac{d^2}{D^2}}Q, \text{ and } \sigma_\varphi(\rho) = -\frac{1+\frac{d^2}{\rho^2}}{1-\frac{d^2}{D^2}}Q, \tag{11}$$

where $d$ and $D$ are inner and outer DP inner diameters, $\rho$ is a variable which is between $D$ and $d$, $F_w$ is the transverse compression force, $S_C$ is the lateral area of the slip body, $K_t$ is the transverse load factor, $\psi$ is the frictional angle, and $Q$, $K_t$ and $\psi$ are given as

$$Q = \frac{F_w}{S_C} = \frac{K_t G}{S_C}, \tag{12}$$

$$K_t = \frac{1}{\tan(\alpha+\psi)}, \tag{13}$$

$$\psi = \tan^{-1}\mu_1. \tag{14}$$

The left hand side of Eq. (9) represents the stress in the DP for extreme axial and radial loads, and when the DP reaches the yield stress, an unrecoverable neck would appear in the clamping region. For the outer surface of the DP, by manipulation of Eqs (9)–(14), the following expression is obtained:

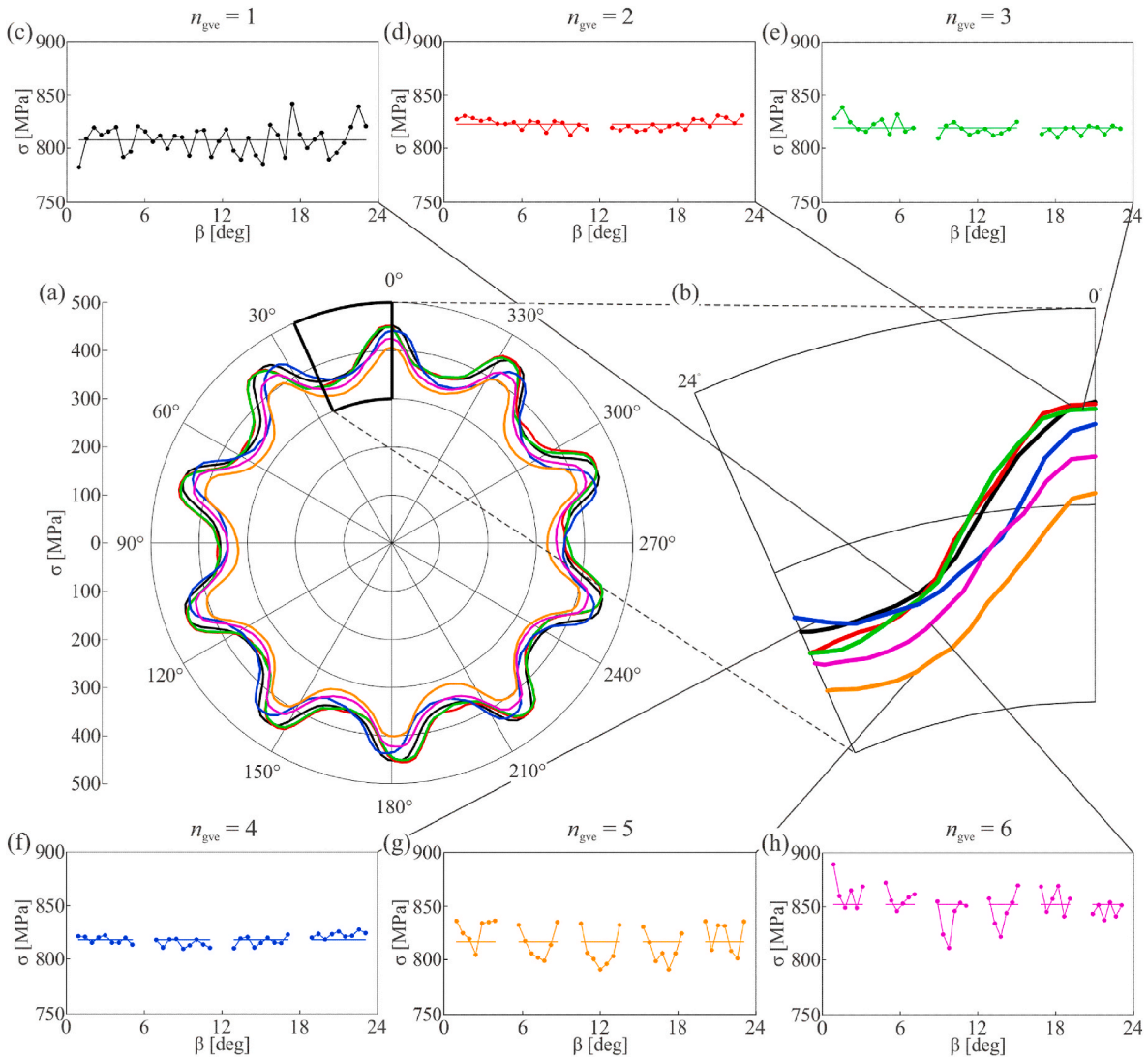


**Fig. 9.** (a) Stress distributions of the DP with respect to the longitudinal groove number: 0 (in black), 1 (in red), 2 (in green), 3 (in blue), 4 (in orange), and 5 (in pink curve) and its zoom (b), showing that the optimized longitudinal groove number is 3. (c)–(h) Stress distributions of the slip inserts with respect to the longitudinal groove number: 0 (in black), 1 (in red), 2 (in green), 3 (in blue), 4 (in orange), and 5 (in pink), showing an optimized groove number is 3 as it has the minimum peak stress as well as a small average stress. (For interpretation of the references to colour in this figure legend, the reader is referred to the Web version of this article.)

$$\left(\frac{G}{S_p}\right)_{outer} = \sqrt{\frac{2}{\left(\frac{2d^2}{D^2-d^2}\frac{K_t S_p}{S_C}\right)^2 + \left(1+\frac{K_t S_p}{S_C}\right)^2 + \left(1+\frac{D^2+d^2}{D^2-d^2}\frac{K_t S_p}{S_C}\right)^2}}\sigma_s, \tag{15}$$

where $\frac{G}{S_p}$ represents the limit axial load that the DP can bear. Similarly for the inner surface of the DP, we have the following expression:

$$\left(\frac{G}{S_p}\right)_{inner} = \sqrt{\frac{2}{\left(\frac{2D^2}{D^2-d^2}\frac{K_t S_p}{S_C}\right)^2 + \left(1+\frac{2D^2}{D^2-d^2}\frac{K_t S_p}{S_C}\right)^2 + 1}}\sigma_s. \tag{16}$$

As can be seen from Equations (15) and (16), $\left(\frac{G}{S_p}\right)_{inner}$ is smaller than $\left(\frac{G}{S_p}\right)_{outer}$, which indicates that the dangerous parts appear on the inner surface of the DP for large clamping load. In this way, when the other parameters are known, the limiting value of the axial gravity load $G$ of the DP that the slip system can withstand can be calculated by using Equation (16). In terms of these theoretical results, the engineers can apply appropriate measures to reduce DP failure in the practical applications.

## 3. Numerical simulation of the DP-slip system

Ideally to comprehensively and robustly assess performance of a DP-slip system, experimental tests with a large number of slips and DPs would be required. However, a such approach is cost prohibitive in most cases and a FE analysis should be used in the first instance. In this section, the FE analysis method is utilized to model and analyze the DP-slip system, and the distribution law of stress in the DP-slip system is obtained.

### 3.1. FE model of the DP-slip system

A 3D model of the DP-slip system developed in ABAQUS using Explicit Module, is shown in Fig. 3(a) depicting its geometry and meshing, where panels (b) and (c) denote the DP and the slip insert, respectively. On average, there are 6 rows and 9 columns with a total of 54 slip inserts in a typical DP-slip system. To reduce simulation time the problem was considered as symmetrical leading to modelling of the stress field for 1 row with 9 slip inserts interacting with a segment of the DP. In the actual slip system operations, a downwards axial impact load is applied on the upper end of the slip inserts before releasing the DP.

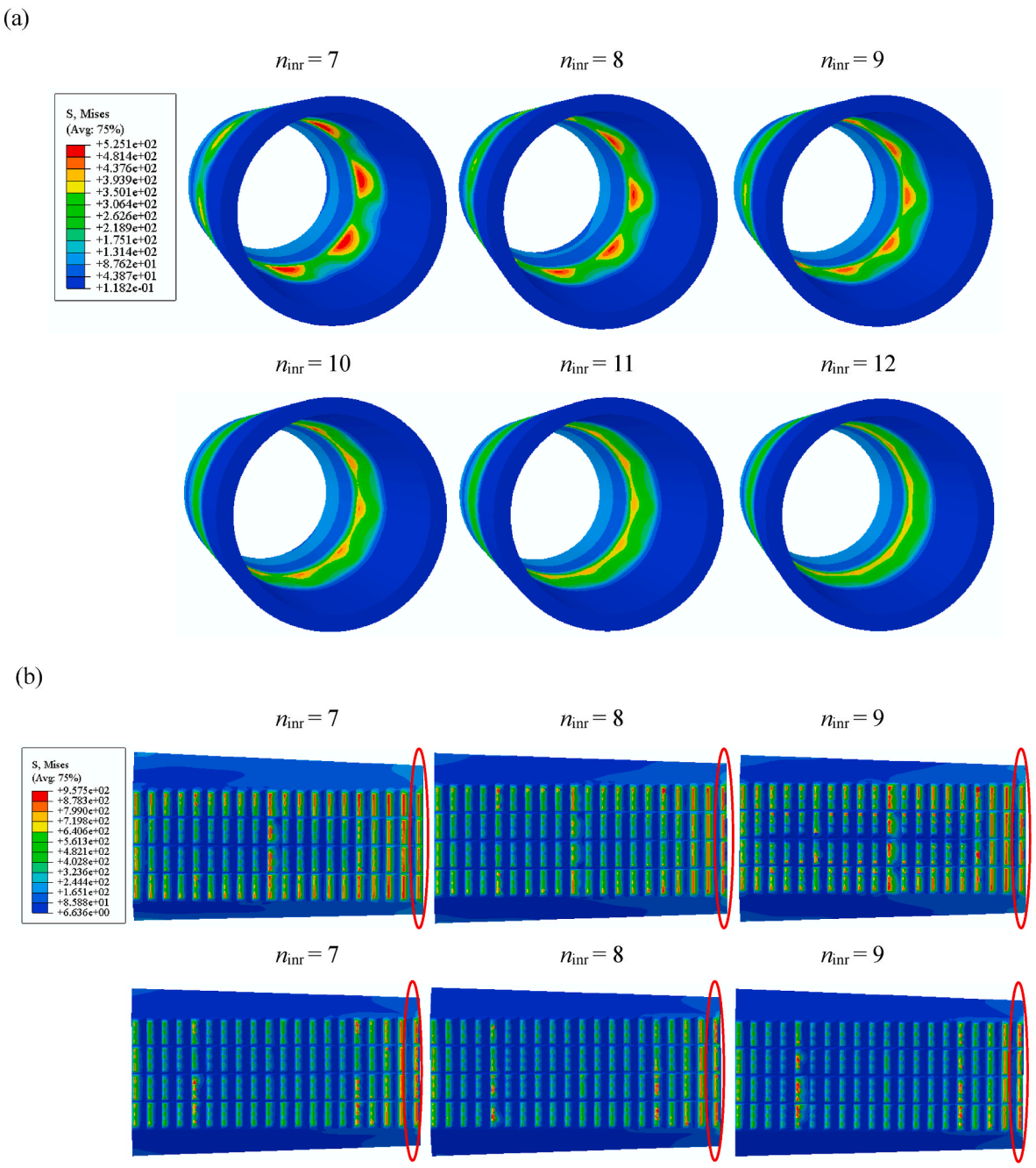


**Fig. 10.** Stress distributions of the DP and slip insert with respect to the number of slip insert which changes from 7 to 12, where the longitudinal groove number is 3 for each slip insert: (a) DP and (b) Slip insert. For the 6 cases, the peak stress of the DP decreases with increasing the number of slip insert. For the slip inserts, the stress of the slip inserts varies significantly and has small peak stress as well as small average stress when the slip insert number is 10 or 11 (Units: MPa).

Thus, the slip inserts can engage with the surface of the DP in advance and the DP can be more reliably clamped by the slip. This method was used in these simulations, which was not addressed in any of the previous research. The total weight of the DP was 180 tons, where 30 tons was applied onto the pipe end of the FE model, an equal share for one row of slip insert. This translates to a pressure of 88.11 MPa applied to the section of the bottom of the DP. In the FE modelling, the element type C3D8R was used for all three parts. It is known that sparse mesh grid lead to fast but less inaccurate results. Although in FE modelling automatic mesh grid generators have been developed to balance the speed and accuracy of the computations, a custom made approach must be used to account for all subtleties of geometry, contact and material properties. As can be seen from Fig. 3, the meshes for contact areas of both the DP and slip insert are refined to improve the simulation accuracy.

For the DP-slip system, the frictional force is the only mechanism that drives the slip bodies downwards, which can be seen from Fig. 2. When a preload is applied, the frictional force between the slip inserts and the DP as well as the frictional force between the slip bodies and the rotary table significantly influence the working capacity of the DP-slip system by clamping the DP. The model presented above assumes the Coulomb friction to describe the contact between the slip bodies and the rotary table as well as the contact between the slip inserts and the DP, with frictional coefficients equal to 0.1 and 0.3, respectively (Sathuvalli et al., 2002; Amezaga et al., 2014). In the FE model, penalty is used as the friction formulation to describe the tangential behaviour. Two analysis

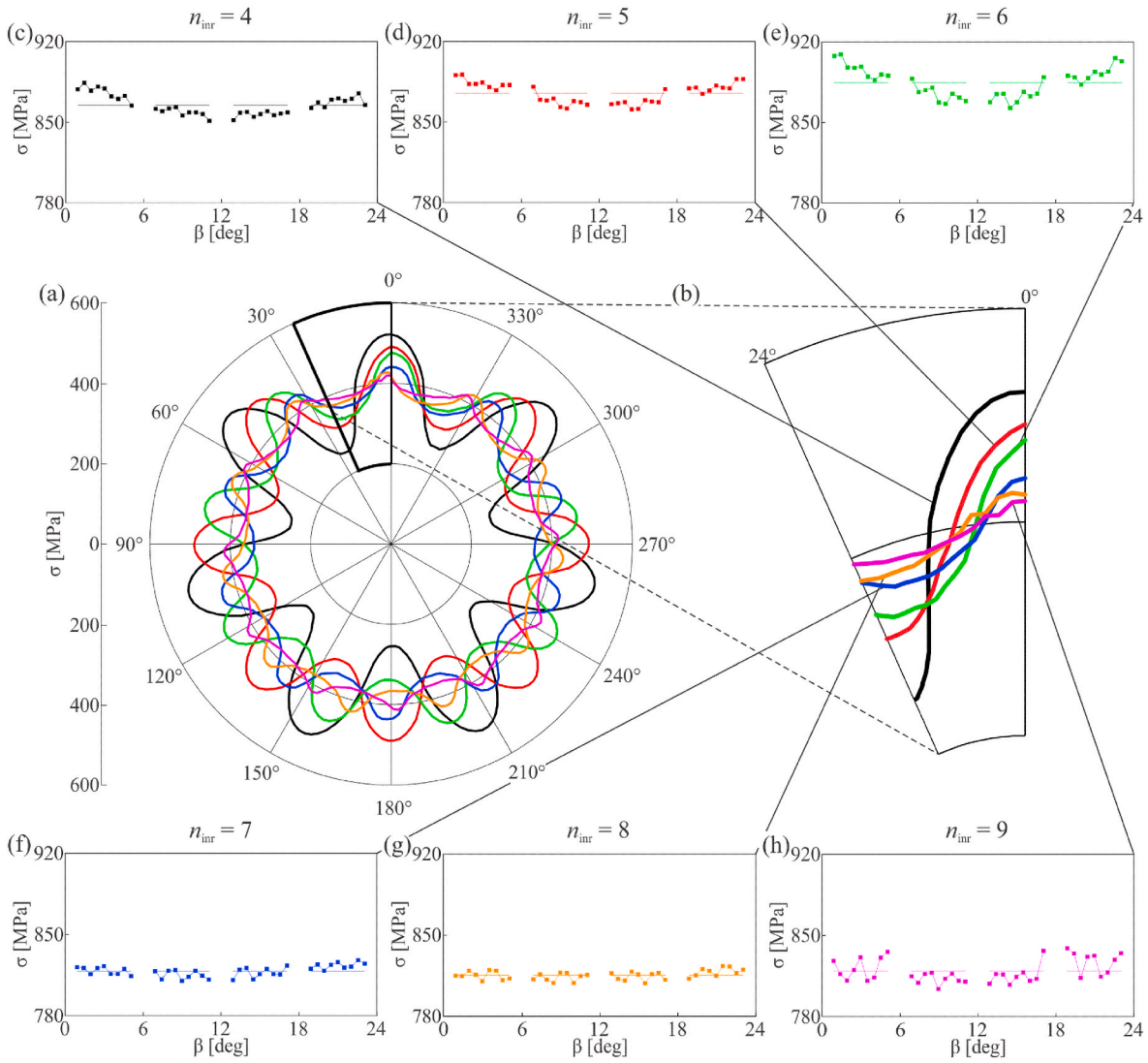


**Fig. 11.** (a) Stress distribution of the DP with respect to the slip insert number: 7 (in black), 8 (in red), 9 (in green), 10 (in blue), 11 (in orange), and 12 (in pink) (d) and its zoom (b), showing that the stress decreases with increasing the number of slip insert. (c)–(h) Stress distribution of the slip inserts with respect to the slip insert number: 7 (in black), 8 (in red), 9 (in green), 10 (in blue), 11 (in orange), and 12 (in pink), showing an optimized groove number is 10 or 11 as the slip insert has small peak stress as well as small average stress. (For interpretation of the references to colour in this figure legend, the reader is referred to the Web version of this article.)

steps are used to load the model and determine the boundary conditions. Boundary conditions and loads are shown in Tables 1 and 2, respectively, whilst the material properties of the FE model are listed in Table 3. In Step 1, we apply a preload to a DP in order to establish a contact between a DP and slip inserts.

### 3.2. Stress responses of the DP-slip system

Based on the FE model presented above, a programme of numerical simulation carried out is presented in this section. For the model, the optimized parameters based on the recent study by Tang et al. (2016) are used directly. Thus, the front rake angle (FRA) is 75°, the back rake angle (BRA) is 35°, the tooth height is 2 mm, and the chamfer is 0.2 mm. By running the FE model, a detailed information on the stress distributions of both slip inserts and DP has been obtained.

Fig. 4 presents the computed stress distributions which show that the DP can be gripped by the slip inserts and a relative sliding doesn't appear, where the overall stress field of the whole system is depicted in Fig. 4 (a). As can be seen from Fig. 4(b), the stress in the middle section of the DP shows higher values than other sections because of the interaction between the DP and slip inserts. For a certain part of the DP, it is interesting that the stress of the inner surface is higher than that of the outer surface, which coincides with the theoretical results presented in Section 2.2 as well as the works conducted by Bai et al. (2016), Wang and Koizumi (2017), Alrsai et al. (2018), and Fernández-Valdés et al. (2020). Fig. 4(c) shows the stress distribution of one of the slip inserts. According to the field experience, slip inserts are prone to fail at two ends. Hence for the purpose of comparison, three positions are investigated including the upper end of the contact section (in black), middle of the contact section (in red), and lower end of the contact section (in blue). Fig. 5(a) shows the stresses at three positions of the slip insert marked in Fig. 4(c) whilst Fig. 5(b) shows the definition of angle β depicted in Fig. 5(a). It is seen from Fig. 5(a) that the stress of the lower region of the slip inserts is the largest. In the figure, the curves are discrete, this is because there are grooves in the slip inserts. For the lower region of the slip insert, the stress value keeps uniform and high. For the upper and middle regions of the slip inserts, however, the stress distributions vibrate frequently along the circumferential direction. This result can be used to explain why some failure phenomenon (plastic deformation, abrasion, and fracture) of the slip insert first appears on its

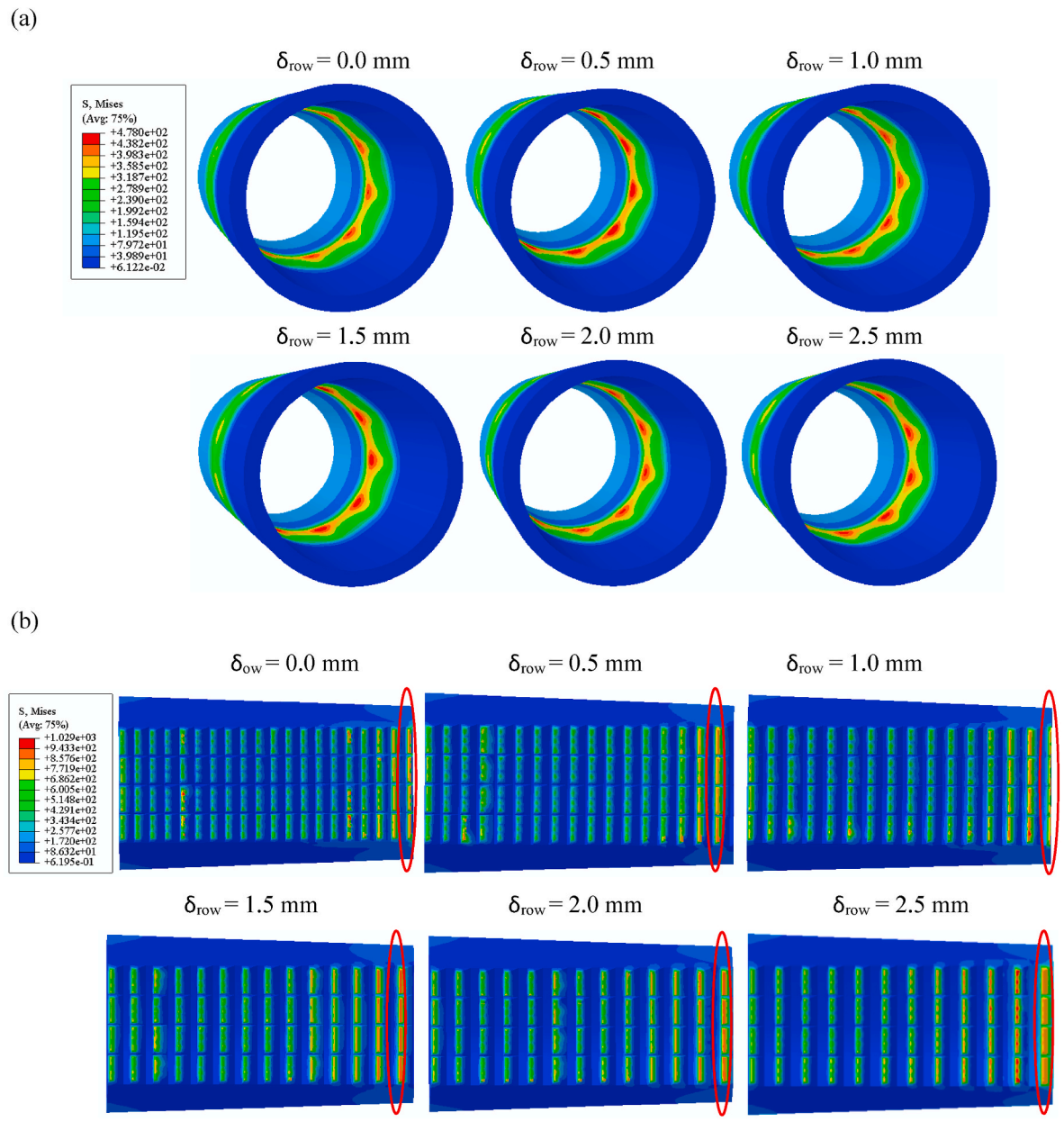


**Fig. 12.** Stress distributions of the DP and slip insert with respect to the row spacing of slip insert, $\delta_{row}$, which changes from 0 to 2.5 mm, where the longitudinal groove number is 3 for each slip insert and the slip insert number is 10: (a) DP and (b) Slip insert. For the 6 cases, the DP reaches its smallest peak stress when the row spacing is 0 mm and highest peak stress when the row spacing is 0.5 mm. For lowest row of the slip insert, the peak stress increases and then decreases and has small peak stress when the row spacing is 0.5 mm (Units: MPa).

edges.

Apart from the stress distribution in different positions of the slip insert, the stress distribution at various locations on the DP is also studied. The stress distribution of the DP-slip system is shown in Fig. 6 in three different of views and the stress of the upper, middle, and lower positions at the contact region of the DP are shown in Fig. 7. For the DP, the three positions are similar to the three positions of the slip insert shown in Fig. 4(c). To get even better insight, the stress distribution of outer surface and inner surface are shown in Fig. 6(a) and (b). In addition, Fig. 6(c) is presented to provide a sectional view of the two surfaces of the DP.

As can be seen from Fig. 7(a) showing the stress distribution on the outer surface of the DP, the DP stresses on the upper, middle, and lower positions of the contact area are distributed in a form of petal. The DP stress along the axial direction of the outer surface is largest in the middle position, which is followed by the lower position and is smallest at the upper position. Meanwhile, the peak stress on the outer surface of the DP occurs in the region, where the slip inserts contact the DP. The stress distribution shown in Fig. 7(a) corresponds to the stress given in Fig. 6(a).

As shown in Fig. 7(b), the stress distribution on the inner surface of the DP is gear-shaped and appears cyclically in the circumferential direction. The DP stress along the axial direction of the inner surface is the largest at the lower position, which is followed by the middle position. The stress curves along the circumferential direction are smooth as there are no zigzag fluctuations, which is contrary to the results shown in Fig. 7(a). Meanwhile, the peak stress of the DP occurs at the inner surface, which corresponds to the gap between the two slip inserts. In general, the distribution of the slip inserts is axisymmetric and the stress distribution on the DP is roughly axisymmetric in the circumferential direction. Stress fluctuations cause the stresses generated by the axial and radial loads to be unevenly distributed over the interaction surface

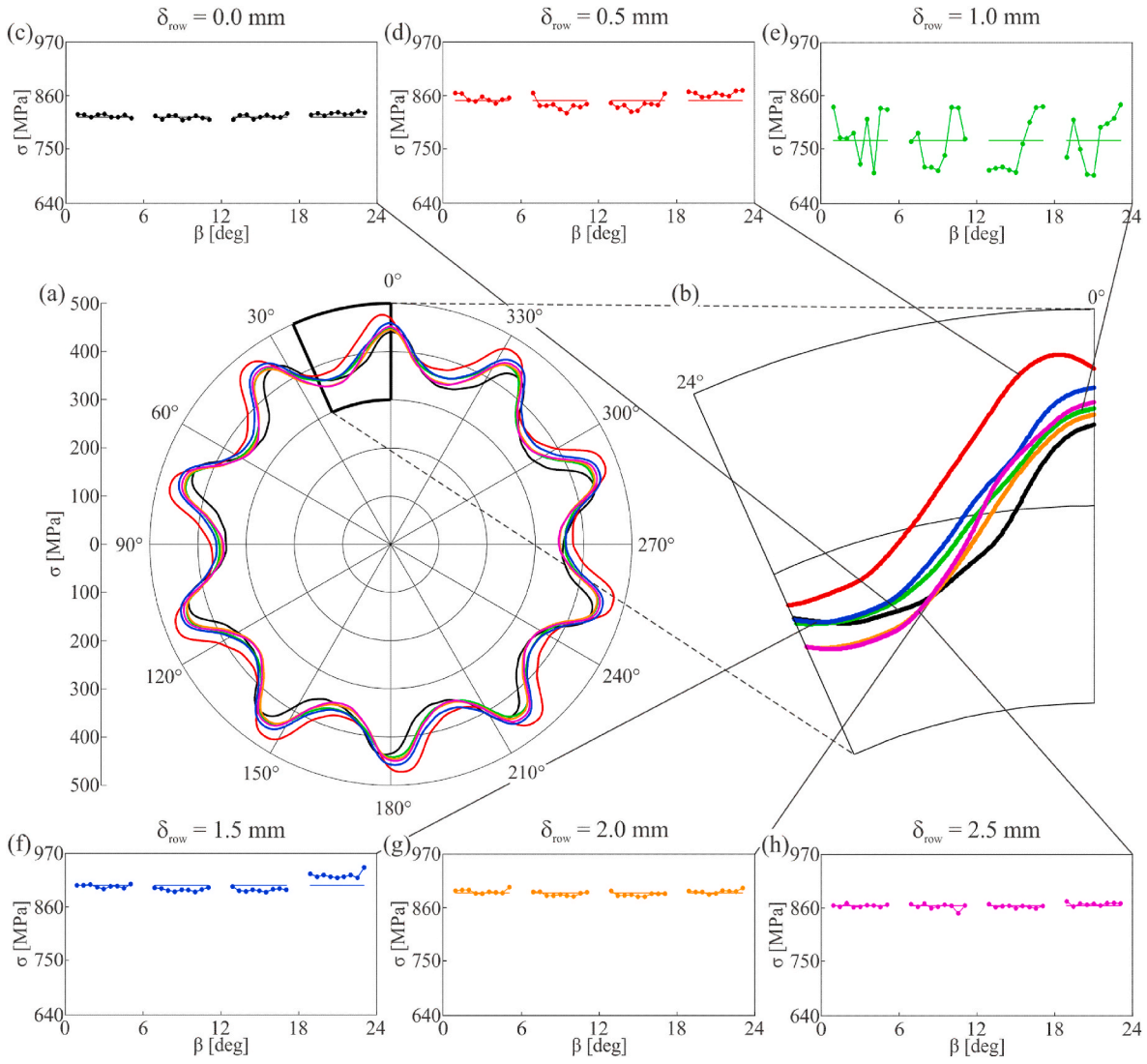


**Fig. 13.** (a) Stress distribution of the DP with respect to the row spacing of the slip insert, $\delta_{row}$: 0 mm (black curve), 0.5 mm (in red), 1 mm (in green), 1.5 mm (in blue), 2 mm (in orange), and 2.5 mm (in pink) and its zoom (b), showing that the DP has a small stress for the case without row spacing. (c)–(h) Stress distribution of the slip inserts with respect to the row spacing of the slip insert: 0 mm (in black), 0.5 mm (in red), 1 mm (in green), 1.5 mm (in blue), 2 mm (in orange), and 2.5 mm (pink), showing that both peak stress as well as average stress of the slip insert reach their smallest values when the row spacing of the slip insert is 0 mm. (For interpretation of the references to colour in this figure legend, the reader is referred to the Web version of this article.)

of the contact area. At the same time, the peak stress of the DP occurs in the contact region and, therefore, is the peak stress on the DP inner surface. For the radial direction positions of the same cross section, the stress on the DP inner surface is significantly greater than that on the outer surface.

## 4. Parametric sensitivity analysis

The results of the parametric sensitivity analysis for the DP-slip system are shown using the following parameters as determined by Tang et al. (2016): FRA of 75°, BRA of 35°, tooth height of 2 mm, and chamfer of 0.2 mm. However, there are many other factors affecting the behavior and performance of slip inserts, for example groove number and row spacing. In this paper, the effects of the longitudinal groove number of the slip insert, the number of slip inserts, and their row spacing on the mechanical behaviors of the DP-slip system are analyzed.

### 4.1. The longitudinal groove number of slip inserts

To date, the effects of the longitudinal groove number of the slip inserts, $n_{gve}$, on the mechanical behavior of the DP-slip are still unknown. This section considers these effects using the FE model described above. Figs. 8 and 9 show the stress distributions of the DP and slip inserts, as the longitudinal groove number of the slip insert, $n_{gve}$, changes from 0 to 5. As seen from Figs. 8(a) and 9(a), an increase in the longitudinal groove number of the slip insert causes the stress of the DP at first remain nearly unchanged, and then decrease before finally increasing. When the longitudinal groove number is from 3 to 5, the maximum stress of the DP has a small value for the 6 cases studied. As shown in Figs 8(b) and 9(c)-(h), the stress has a small average stress for the case without longitudinal groove and large average stress when the groove number is 5. When the longitudinal groove number is from 3 to 5, the average stress seems to keep constant. When regarding to the peak stress, however, the stress is more uniform when the groove number is 3. By combining the stress distributions of the DP and slip insert, an optimized value for the groove number is 3.

### 4.2. The number of slip inserts

The effect of the number of slip inserts, $n_{inr}$, on the mechanical

behavior of the slip insert-DP system is studied, with the slip insert number changing from 7 to 12. Figs 10 and 11 show the stress distribution of the DP and slip insert with respect to the number of slip insert, $n_{inr}$, when the longitudinal groove number is 3 for each slip insert. As seen from Figs 10(a) and 11(a), with an increase in the number of slip insert, $n_{inr}$, the peak stress of the DP decreases gradually. In general, the maximum stress of the DP has a small value when the number of the slip inserts is from 10 to 12 for the 6 cases studied. For the slip inserts, it is shown in Figs 10(b) and 11(c)-(h), that the stress of the slip inserts varies significantly for the 6 cases studied. Considering the stress of the DP, and stress of the slip insert, the suggested number of slip inserts is 10 or 11.

### 4.3. Row spacing of the slip insert

The row spacing, $\delta_{row}$, is another important factor for the slip insert structure. Based on the field experience and the existing structure of the slip insert, the row spacing, $\delta_{row}$, changes from 0 to 2.5 mm in steps of 0.5 mm. Figs. 12 and 13 show the stress distribution of the DP and slip insert with respect to the row spacing of slip insert which changes from 0 to 2.5 mm. As shown in Figs 12(a) and 13(a), the DP reaches its smallest peak stress when the row spacing is 0 mm and highest peak stress when the row spacing is 0.5 mm. For the stress of the slip insert shown in Figs 12(b) and 13(c)-(h), its smallest peak stress as well as average stress are reached when the row spacing is 0 mm. Combining with the stress of the DP and slip insert, 0 mm is an optimal value for the row spacing of the slip insert.

## 5. Conclusions

In this paper, a DP-slip system has been studied in detail through a combination of theoretical and FE analysis. The model has been set up in a way to take into account the properties of an actual DP-slip system, particularly regarding the typical materials, geometric dimensions, loads and adequate boundary conditions. It is found that the frictional coefficient $\mu_1$ between the slip body and the rotary table significantly influences the radial load distribution on the DP and the ability of the slip to clamp it in place. The theoretical model developed in this paper confirms that the DP can be securely clamped using the slip system for a small value of a frictional coefficient $\mu_1$, but the DP will carry a larger radial load as a consequence. Therefore, the value of $\mu_1$ should be considered comprehensively in practical applications. By comparing the ultimate axial load that the inner and outer surfaces of the DP can bear, the results presented in this paper show that the dangerous zones appear on the inner surface of the DP, which itself is consistent observations from the drilling field.

The simulation results indicate that the stresses generated by the axial and radial loads are not uniformly distributed on the contact area between the DP and the slip inserts, but instead are concentrated within certain areas. The maximum stress of the inner surface of the DP occurs in the gap between each the two slip inserts, making the stress of the inner surface of the DP oscillate periodically along its circumference. For the stress distribution of the slip insert, the maximum stress occurs at its lower end, which can be of interest to manufacturers to pay more attention to the processing quality of the lower end of the slip.

The parametric sensitivity analysis carried out in this work, considers the effects of the longitudinal groove number of the slip inserts, the number of the slip inserts, and the row spacing of the slip insert on the mechanical behavior of the whole DP-slip system. By comparing the stress distributions of the DP as well as the slip insert, the optimized values of the longitudinal groove number of the slip inserts, the number of slip inserts, and the row spacing of the slip insert can be identified as 3, 10, and 0, respectively.

## CRediT author statement

**Lipping Tang:** Investigation, Methodology, Validation, Writing-Original draft preparation; **Baolin Guo:** Investigation, Calculation, Writing- Original draft preparation; **Marcin Kapitaniak:** Software, Investigation, Visualization, Writing- Original draft preparation, **Vahid Vaziri:** Software, Investigation, Writing- Original draft preparation, Editing; **Marian Wiercigroch:** Conceptualization, Methodology, Writing- Reviewing, Supervision, Editing.

## Declaration of competing interest

The authors declare that they have no known competing financial interests or personal relationships that could have appeared to influence the work reported in this paper.

## Data availability

No data was used for the research described in the article.

## Acknowledgments

This research is supported by the National Natural Science Foundation of China (No. 51904262), the China Postdoctoral Science Foundation (No. 43XB3793XB), and the State Scholarship Fund of the China Scholarship Council (No. 201808515055).

## References

Adeosun, O.A., Tabash, M.I., Anagreh, S., 2022. Oil price and economic performance: additional evidence from advanced economies. Resour. Pol. 77, 102666.
Albdiry, M.T., Almensory, M.F., 2016. Failure analysis of drillstring in petroleum industry: a review. Eng. Fail. Anal. 65, 74–85.
Alrsai, M., Karampour, H., Albermani, F., 2018. On collapse of the inner pipe of a pipe-in-pipe system under external pressure. Eng. Struct. 172, 614–628.
Ali, J.A., Kalhury, A.M., Sabir, A.N., Ahmed, R.N., Ali, N.H., Abdullah, A.D., 2020. A state-of-the-art review of the application of nanotechnology in the oil and gas industry with a focus on drilling engineering. J. Petrol. Sci. Eng. 191, 107118.
Amezaga, F., Rials, J.R., Heidecke, K., 2014. Landing string slip system: state-of-the-art design to minimise pipe crushing problems. In: Proceedings of the SPE Asia Pacific Oil & Gas Conference and Exhibition. Adelaide, Australia.
Awad, A., Carrois, F., Lafuente, M., Matveyev, A., 2019. Design and comparison of two drill string solutions that break barriers in extend reach drilling. In: Proceedings of the SPE/IADC International Conference and Exhibition. Netherland, Hague.
Bai, Y., Liu, T., Cheng, P., Yuan, S., Yao, D., Tang, G., 2016. Buckling stability of steel strip reinforced thermoplastic pipe subjected to external pressure. Compos. Struct. 152, 528–537.
Belkacem, L., Abdelbaki, N., Otegui, J.L., Gaceb, M., Bettayeb, M., 2019. Using a superficially treated 2024 aluminum alloy drill pipe to delay failure during dynamic loading. Eng. Fail. Anal. 104, 261–273.
Bordet, L., Franchi, J., Granger, S., Vierke, A., 2016. Innovative forging process allows safer and cost effective heavy duty landing string for deepwater applications. In: Proceedings of the SPE Deepwater Drilling and Completions Conference. Galveston, Texas.
Boresi, A.P., Chong, K.P., 2011. Elasticity in Engineering Mechanics, third ed. John Wiley and Sons Inc, New York.
Brock, J.N., Chandler, R.B., Jellison, M.J., Sanclemente, L.W., Robichaux, R.J., Saleh, M., 2007. 2 million-lbm slip-based landing string system pushes the limit of deepwater casing running. In: Proceedings of the Offshore Technology Conference. Houston, Texas.
Chang, Y., Jiang, Y., Zhang, C., Xue, A., Chen, B., Zhang, W., Xu, L., Liu, X., Dai, Y., 2021. PERT based emergency disposal technique for fracture failure of deepwater drilling riser. J. Petrol. Sci. Eng. 201, 108407.
Damjanović, D., Kozak, D., Gubeljak, N., 2019. The influence of residual stresses on fracture behavior of pipe ring notched bend specimen (PRNB). Eng. Fract. Mech. 205, 347–358.
Dao, N.H., Sellami, H., 2012. Stress intensity factors and fatigue growth of a surface crack in a drill pipe during rotary drilling operation. Eng. Fract. Mech. 96, 626–640.
Falcone, G., Liu, X., Okech, R.R., Seyidov, F., Teodoriu, C., 2018. Assessment of deep geothermal energy exploitation methods: the need for novel single-well solutions. Energy 160, 54–63.
Feng, L., Qian, X., 2020. Enhanced crack sizing and life estimation for welded tubular joints under low cycle actions. Int. J. Fatig. 137, 105670.
Fernández-Valdés, D., Vázquez-Hernández, A.O., Ortega-Herrera, J.A., Ocampo-Ramírez, A., Hernández, D., 2020. FEM-based evaluation of friction and initial imperfections effects on sandwich pipes local buckling. Mar. Struct. 72, 102769.
Flores, V., Franchi, J., Granger, S.L., Vierke, A., 2015. Innovative heavy landing system for ultra deep offshore: extended slip crush resistant tube, enhanced slip design and heavy weight carrier. In: Proceedings of the 12th Offshore Mediterranean Conference and Exhibition. Italy, Ravenna.

Hayatdavoudi, A., 1985. Elastic yield of casing due to elevator/spider system. In: Proceedings of the IADC/SPE Drilling Conference. Louisiana, New Orleans.
Hill, T., Ellis, S., Lee, K., Reynolds, Nicholas, Zheng, N., 2004. An innovative design approach to reduce drill string fatigue. In: Proceedings of the IADC/SPE Drilling Conference. Dallas, Texas.
Hossain, M.M., Rahman, M.K., Rahman, S.S., Akgun, F., Kinzel, H., 1998. Fatigue life evaluation: a key to avoid drill pipe failure due to die-marks. In: Proceedings of the IADC/SPE Asia Pacific Drilling Technology. Jakarta, Indonesia.
Jarski, J.M., Yousef, F.J., Vandervort, K., Campbell-smith, G., 2011. Development of ball-and-pocket gripping technology to overcome slip handling limitations. In: Proceedings of the SPE Offshore Europe Oil and Gas Conference and Exhibition. Aberdeen, UK.
Liu, G., 2021. Challenges and countermeasures of log evaluation in unconventional petroleum exploration and development. Petrol. Explor. Dev. 48, 1033–1047.
Li, X., Jiang, X., Hopman, H., 2018. A review on predicting critical collapse pressure of flexible risers for ultra-deep oil and gas production. Appl. Ocean Res. 80, 1–10.
Li, Z., Zhang, C., Song, G., 2017. Research advances and debates on tubular mechanics in oil and gas wells. J. Petrol. Sci. Eng. 151, 194–212.
Liu, F., Zhou, S., Xia, C., Zeng, D., Shi, T., 2016. Optimization of fatigue life distribution model and establishment of probabilistic S-N curves for a 165 ksi grade super high strength drill pipe steel. J. Petrol. Sci. Eng. 145, 527–532.
Liu, W., Li, J., Zhong, Y., Shi, T., Zhang, J., Li, S., 2022. Failure analysis on aluminum alloy drill pipe with pits and parallel transverses cracks. Eng. Fail. Anal. 131, 105809.
Lu, S., Feng, Y., Luo, F., Qin, C., Wang, X., 2005. Failure analysis of IEU drill pipe wash out. Int. J. Fatig. 27, 1360–1365.
Moradi, S., Ranjbar, K., 2009. Experiment and computation failure analysis of drillstrings. Eng. Fail. Anal. 16, 923–933.
Paslay, P., Pattillo, P.D., Pattillo, D., Sathuvalli, U.B.R., Payne, M.L., 2006. A re-examination of drillpipe/slip mechanics. In: Proceedings of the IADC/SPE Drilling Conference (Miami, USA).
Payne, M.L., Pattillo, P.D., Driscoll, P.M., Sathuvalli, U.B., 2005. Experimental investigation of drillpipe loaded in slips. In: Proceedings of the World Tribology Congress III. Washington, USA.
Rahman, M.K., Hossain, M.M., Rahman, S.S., 1999a. Stress concentration incorporated fatigue analysis of die-marked drill pipes. Int. J. Fatig. 21, 799–811.
Rahman, M.K., Hossain, M.M., Rahman, S.S., 1999b. Survival assessment of die-marked drill pipes: integrated static and fatigue analysis. Eng. Fail. Anal. 6, 277–299.
Reinhold, W.B., Spiri, W.H., 1959. Why does pipe fail in the slip area? World Oil 100.
Santus, C., Burchianti, A., Inoue, T., Ishiguro, H., 2020. Fatigue resonant tests on S140 and S150 grade corroded drill pipe connections and pipe bodies. Int. J. Pres. Ves. Pip. 185, 104104.
Sathuvalli, U.B., Payne, M.L., Suryanarayana, P.V., Shepard, J., 2002. Advanced slip crushing considerations for deepwater drilling. In: Proceedings of the IADC/SPE Drilling Conference. Dallas, Texas.
Shahani, A.R., Sharifi, S.M.H., 2009. Contact stress analysis and calculation of stress concentration factors at the tool joint of a drill pipe. Mater. Des. 30, 3615–3621.
Sikder, A., Inekwe, J., Bhattacharya, M., 2019. Economic output in the era of changing energy-mix for G20 countries: new evidence with trade openness and research and development investment. Appl. Energy 235, 930–938.
Simpson, B.R., Payne, M.L., Jellison, M.J., Adams, B.A., 2005. 2,000,000-lbf landing-string developments: novel slipless technology extends the deepwater operating envelope. SPE Drill. Complet. 20, 109–122.
Sun, Y., Zhang, F., Wang, Q., Gao, K., 2016. Application of “crust 1” 10k ultra-deep scientific rig in Songliao basin drilling project (CCSD-SKII). J. Petrol. Sci. Eng. 145, 222–229.
Tang, L., Guo, B., Zhu, X., 2020. Finite element modeling of slip insert geometric grip optimization for oil well drill pipes. Math. Probl Eng. 2020, 5426739.
Tang, L., Zhu, X., Li, J., Shi, C., 2016. Optimization analysis on the effects of slip insert design on drill pipe damage. J. Fail. Anal. Prev. 16, 384–390.
Tikhonov, V., Gelfgat, M., Ring, L., Bukashkina, O., 2017. Refinement of the drill pipe-slip mechanical model. In: Proceedings of the SPE Russian Petroleum Technology Conference. Moscow, Russia.
Tomac, I., Sauter, M., 2018. A review on challenges in the assessment of geomechanical rock performance for deep geothermal reservoir development. Renew. Sustain. Energy Rev. 82, 3972–3980.
Verhoef, R., Rijzingen, H., 2015. Tested and confirmed: the 1250-ton slip-proof landing string and slip system. In: Proceedings of the SPE/IADC Drilling Conference and Exhibition. London, United Kingdom.
Vreeland Jr., T., 1961. Deformation of drill pipe held in rotary slips. In: Proceedings of the Petroleum Mechanical Engineering Conference. Kansas City, Missouri.
Wang, J.H., Koizumi, A., 2017. Experimental investigation of buckling collapse of encased liners subjected to external water pressure. Eng. Struct. 151, 44–56.
Zaman, K., Moemen, M.A., 2017. Energy consumption, carbon dioxide emissions and economic development: evaluating alternative and plausible environmental hypothesis for sustainable growth. Renew. Sustain. Energy Rev. 74, 1119–1130.
Zamani, S.M., Hassanzadeh-Tabrizi, S.A., Sharifi, H., 2016. Failure analysis of drill pipe: a review. Eng. Fail. Anal. 59, 605–623.
Zhang, H., Gao, D., Tang, H., 2010. Choice of landing string under ultra-deepwater drilling condition. In: Proceedings of the CPS/SPE International Oil and Gas Conference and Exhibition. Beijing, China.
Zhang, Z., Zhu, X., 2020. Failure analysis and improvement measures of step transition zone of drill pipe joint. Eng. Fail. Anal. 109, 104211.